phys. stat. sol. (a) **205**, No. 4, 837–840 (2008) / **DOI** 10.1002/pssa.200777747

physica status solidi a
www.pss-a.com
applications and materials science

Optical characterization of rocksalt $Pb_{1-x}Sn_xTe$ alloys

Nilton Souza Dantas[*, 1, 2, 3], **Hans Arwin**[4], **Gabriel Nzulu**[4], **Paulo Henrique de Oliveira Rappl**[3], **Antônio Ferreira da Silva**[5], **and Clas Persson**[1]

[1] Department of Materials Science and Engineering, Royal Institute of Technology, 100 44 Stockholm, Sweden
[2] Área de Informática, Departamento de Ciências Exatas, Universidade Estadual de Feira de Santana, 44031-460 Feira de Santana, Ba, Brazil
[3] Instituto Nacional de Pesquisas Espaciais, INPE/LAS-C.P. 515, 12210-970 São José dos Campos, SP, Brazil
[4] Laboratory of Applied Optics, Department of Physics, Chemistry and Biology, Linköping University, 58 183 Linköping, Sweden
[5] Instituto de Física, Universidade Federal da Bahia, Campus Universitário de Ondina, 40210-340 Salvador, Ba, Brazil

Received 8 June 2007, revised 30 January 2008, accepted 31 January 2008
Published online 26 March 2008

PACS 71.20.Nr, 78.20.Ci, 78.40.Fy

* Corresponding author: e-mail nilton@uefs.br

The optical properties in terms of dielectric function $\varepsilon(\hbar\omega) = \varepsilon_1(\hbar\omega) + i\varepsilon_2(\hbar\omega)$ of rocksalt $Pb_{1-x}Sn_xTe$ alloys ($0 \le x \le 1$) are investigated experimentally by spectroscopic ellipsometry and theoretically by first-principles electronic band structure calculation. We find a strong optical response in the 0.5–2.0 eV region arising from optical absorption around the LW-line of the Brillouin zone. The response peak of the imaginary part of the dielectric functions at $E = 1.6$–1.8 eV shifts towards lower energies for high Sn compositions as a consequence of narrower W-point band-gap $E_g(W)$ for the Sn-rich alloys.

1 Introduction The lead-tin telluride alloys, $Pb_{1-x}Sn_xTe$, are narrow bandgap group-IV–VI semiconductors with NaCl-like crystalline structure. By vary-ing the Sn concentration x from 0 to 1, the direct band-gap energy at the L-point changes non-linearly from $E_g(PbTe) \approx 0.18$ eV to $E_g(SnTe) \approx 0.30$ eV, in which the gap occurs at or near the L-point, with $E_g(Pb_{1-x}Sn_xTe) \approx 0$ eV for $x \approx 0.30$ at low temperatures [1, 2]. This interesting electronic property of $Pb_{1-x}Sn_xTe$ is used when designing infrared photo detectors [3], diode lasers [4], and thermophotovoltaic energy converters [5]. In this work, we use spectroscopic ellipsometry in the spectral range 0.7–6.5 eV to investigate the linear optical response of $Pb_{1-x}Sn_xTe$ alloys in terms of the complex dielectric function $\varepsilon = \varepsilon_1 + i\varepsilon_2$ versus the photon energy $\hbar\omega$. Eleven samples of $Pb_{1-x}Sn_xTe$ ($0 \le x \le 1$) of p-type were grown through molecular beam epitaxy (MBE). Theoretically, we employ the first-principles full-potential linearized augmented plane wave (FPLAPW) method [8] within the local density approximation (LDA) and with a full relativistic Hamiltonian. The $Pb_{1-x}Sn_xTe$ alloy ($x = 0.0$, 0.25, 0.50, 0.75 and 1.0) is modeled by an eight atoms conventional unit cell. Both the calculated dielectric function $\varepsilon(\hbar\omega)$ and absorption coefficient $\alpha(\hbar\omega)$ are presented and compared with the experimental $\varepsilon(\hbar\omega)$ spectra.

2 Sample preparation Eleven samples of p-type $Pb_{1-x}Sn_xTe$ ($x = 0.0$, 0.1, . . ., 1.0) were grown in a Riber 32P MBE machine, on freshly cleaved BaF_2 (111) substrates having an area of 15×15 mm^2. The variable Sn contents of the ternary alloys was obtained by adjusting the flux ratio between two separate effusion cells, respectively containing solid sources of the binary compounds PbTe and SnTe, which sublimate mainly as molecules. Since $Pb_{1-x}Sn_xTe$ has a p-type conductivity character only for $x > 0.25$, with a high density (10^{19}–10^{20} cm^{-3}) of carriers, Te_2 from an additional effusion cell was used to make sure that all samples were p-type, particularly those with $x < 0.25$. The background pressure in the growth chamber was kept below 10^{-9} Torr. The nominal composition x of the epitaxial film was estimated from the ratio between the beam equivalent pressures (BEP) of PbTe and SnTe [6],

whose partial pressures were separately measured by an ion gauge placed at the substrate position, prior and after the growth. For growing this series of samples, the total (PbTe + SnTe) BEP was kept fixed at 4.6×10^{-6} Torr, while the Te_2 BEP was varied from 8.5×10^{-8} down to zero Torr, as x went from 0 to 1. The nominal substrate temperature was kept at 208 °C, as measured by a thermocouple in the back side of the molybdenum block which held the BaF_2 substrates. Due to optical measurement requirements, the layer thickness was kept about 2 μm for all samples. As estimated by their RHEED pattern, the surfaces of all epilayers were almost atomically flat.

3 Experimental details Spectroscopic ellipsometry was used for determination of the spectral dependence of the complex dielectric function ε versus photon energy $\hbar\omega$. The measurements were performed in air using a variable angle of incidence ellipsometer from J. A. Woollam Co. in the photon energy range 0.73–6.5 eV at the angles of incidences 50, 60, 70 and 80 degrees. The samples were found to have surface layers which so far not are fully characterized; the simple modeling indicates roughness as the main overlayer, possibly intermixed with some oxide. The total thickness varied among the samples and was in the range 5–12 nm. However, from the present measurements it was not possible to extract the detailed properties of these overlayers and a surface roughness of 8 nm was assumed for all samples. The measured ellipsometry data were thus evaluated in a three-phase model with a substrate, a roughness layer and an air ambient. The roughness layer was modeled with the Bruggeman effective medium approximation [7] assuming 50% air and 50% bulk material and a fixed thickness of 8 nm, and the complex-valued bulk dielectric function $\varepsilon(\hbar\omega) = \varepsilon_1(\hbar\omega) + i\varepsilon_2(\hbar\omega)$ was fitted on a wavelength-by-wavelength basis using all angles of incidence.

4 Computational details Theoretically, we employ the first-principles FPLAPW method [8] within the LDA, and with a full relativistic Hamiltonian; that is, the core states are treated fully relativistic and including spin–orbit interaction as a perturbation to the scalar-relativistic self-consistent field calculation. A detailed description of the electronic band structure of PbSn and PbTe are found in [9]. In that work, we also show how the spin–orbit interaction affects the band structure and its pressure coefficients. The $Pb_{1-x}Sn_xTe$ alloy is modeled by an eight atoms conventional NaCl-like unit cell. This $Pb_{4-n}Sn_nTe_4$ cells ($n = 0$, 1, . . ., 4) represent thus $x = 0.0$, 0.25, 0.50, 0.75, and 1.0, and has thus periodic sublattices of the Pb and Sn atoms. We use experimental lattice constants for the PbTe and SnTe binaries [8] and applying the Vegard's law for the alloys, which is justified by the experimental lattice constant of NaCl-like $PbSnTe_2$ [10] as well as with our pseudopotential volume optimization of $Pb_{4-n}Sn_nTe_4$ [11]. The all-electron potential is converged with 64 $\boldsymbol{k}$-points in the irreducible Brillouin zone (BZ) and with $R_{mt} \cdot K_{max} = 8$, where $R_{mt} = 1.53$ Å is the muffin-tin radius of the cations as well as of the anions; this corresponds to about 650 plane waves. The imaginary part $\varepsilon_2(\hbar\omega)$ of the dielectric function is obtained from the electronic structure through the joint density-of-states and the momentum matrix elements $\boldsymbol{p}$ (in the long wavelength limit, i.e. $\boldsymbol{q} \to 0$) [12]:

$$\varepsilon_2^{ij}(\hbar\omega) = \frac{4\hbar\pi^2 e^2}{\Omega m^2 \omega^2} \sum_{knn'} \langle \boldsymbol{kn}| p_i |\boldsymbol{kn}'\rangle \langle \boldsymbol{kn}'| p_j |\boldsymbol{kn}\rangle \times f_{\boldsymbol{kn}}(1 - f_{\boldsymbol{kn}'})\, \delta(E_{\boldsymbol{kn}'} - E_{\boldsymbol{kn}} - \hbar\omega)\,, \quad (1)$$

with a denser mesh of 343 $\boldsymbol{k}$-points in the irreducible BZ. Here, $f_{\boldsymbol{kn}}$ is the Fermi distribution, e is the electron charge, m its mass, Ω is the volume of unit cell, and $|\boldsymbol{kn}\rangle$ is the crystal wave function corresponding to the n-th eigenvalue $E_{\boldsymbol{kn}}$ with wave vector $\boldsymbol{k}$. The real part $\varepsilon_1(\hbar\omega)$ of dielectric function is obtained from the Kramers–Kroning transformation relation [12].

5 Results and discussion The measured ellipsometry data are presented in Fig. 1. The real part of the dielectric function (Fig. 1(a)) shows for Sn-rich compounds a

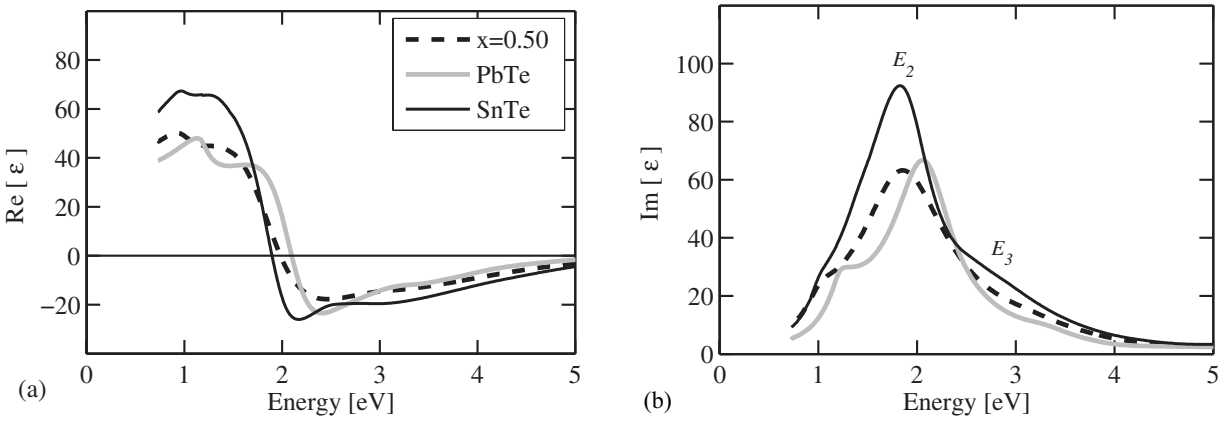

Figure 1 Measured optical response $\langle \varepsilon(\hbar\omega) \rangle = \langle \varepsilon_1(\hbar\omega) \rangle + i\langle \varepsilon_2(\hbar\omega) \rangle$ by spectroscopic ellipsometry.

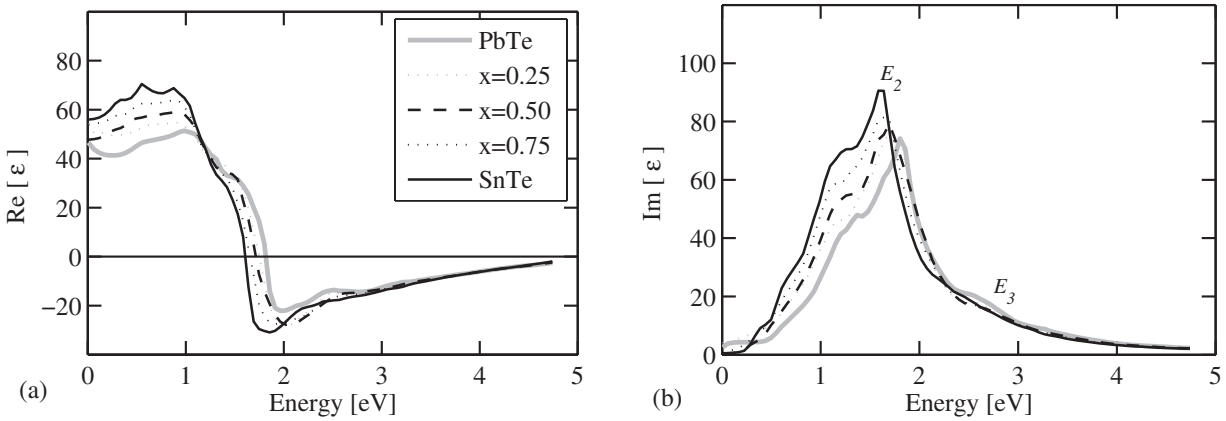

Figure 2 Calculated (a) real and (b) imaginary parts of the dielectric function $\varepsilon(\hbar\omega) = \varepsilon_1(\hbar\omega) + i\varepsilon_2(\hbar\omega)$ for $Pb_{1-x}Sn_xTe$, using a fully relativistic FPLAPW/LDA method with a small Lorentz broadening of 0.02 eV.

larger value in the 0.7–1.5 eV region. The Sn-rich spectra shift towards lower photon energies near $\hbar\omega \approx 2$ eV. This shift towards lower energies for Sn-rich compounds is also apparent in the imaginary part of the dielectric function (Fig. 1(b)). The main structures in the spectra are labeled E_1 and E_3, as proposed in [13]. The spectra indicate a "knee" at about 1–1.2 eV which is more apparent for the Pb-rich compounds.

The calculated dielectric function (Fig. 2) agrees rather well with measured spectra. The LDA is well-known to underestimate the band-gap energy [9] and therefore the position of E_0 critical point is not shown in the theoretical spectra. However, normally the trends in the band gaps and optical properties are accurate within full-potential LDA. The strong optical response in the interval 0.5–2.0 eV (Fig. 2(b)) represents the optical absorption mainly in the LW region of the BZ. The shift of the peak energy E_2 towards lower energies for high Sn compositions is a consequence of smaller band gap E_g at the W-point: $E_2 = 1.81$, 1.72, 1.66, 1.64, and 1.59 eV and $E_g(W) = 1.86$, 1.73, 1.76, 1.61 and 1.61 eV for $x = 0.00$, 0.25, 0.50, 0.75, and 1.00, fore these compositions have a stronger response in the

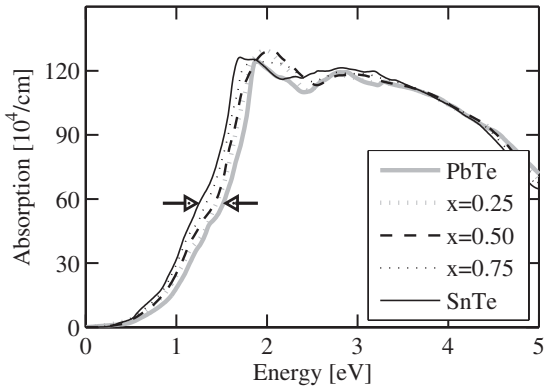

Figure 3 Determined absorption coefficient $\alpha(\hbar\omega)$ obtained from the calculated $\varepsilon(\hbar\omega)$ in Fig. 2. The arrows indicate the difference of 0.27 eV in photon energy at $\alpha(\hbar\omega) = 60 \times 10^4$/cm.

1 eV region. The calculated "knee" (cf. Fig. 1(b)) at about respectively. Sn-rich alloys have more flat curvature of the lowest conduction band along the LW-line [9], and there 1–1.5 eV appears for both Pb- and Sn-rich compounds. The calculated absorption coefficient [Fig. 3] shows also an energy shift towards lower energies for the Sn-rich alloys; the shift between PbTe and SnTe is about 0.27 eV for $\alpha(\hbar\omega) = 60 \times 10^4$/cm. The details in the spectra in the lower energy region ($\hbar\omega < 0.3$ eV) cannot be analyzed by the LDA due to incorrect order of the eigenfunction symmetries of the band edges at the L-point [9].

6 Conclusion We have investigated the optical properties of $Pb_{1-x}Sn_xTe$ alloy using ellipsometry measurements and theoretically using the FPLAPW method. The measured and calculated complex dielectric functions agree well. The strong optical response in the 0.5–2.0 eV region arises from optical band-to-band absorption around the LW symmetry line. The response peak (in imaginary part of dielectric function) at $E_2 = 1.6$–1.8 eV shifts towards lower energies for high Sn compositions as a consequence of narrower W-point band-gap $E_g(W)$ for the Sn-rich alloys: $E_g(W; PbTe) - E_g(W; SnTe) = 0.27$ eV.

Acknowledgments This work was financially supported by the Swedish Institute (SI), the Swedish Foundation for International Cooperation in Research and Higher Education (STINT), the Swedish Research Council (VR), Brazilian Agencies FAPESB (Bahia), CNPq and REMAN/CNPq.

References

[1] J. O. Dimmock, I. Melngailis, and A. J. Strauss, Phys. Rev. Lett. **16**, 1193 (1966).
[2] E. Abramof, S. O. Ferreira, P. H. O. Rappl, H. Closs, and I. N. Bandeira, J. Appl. Phys. **82**, 2405 (1997).
[3] Y. Horikoshi, in: Semiconductors and Semimetals, Vol. 22, part C, edited by W. T. Tsang (Academic, New York, 1985), p. 93.
[4] H. Preier, Appl. Phys. **20**, 189 (1979).

[5] T. K. Chaudhuri, Int. J. Energy Res. **16**, 481 (1998).
[6] P. H. O. Rappl, H. Closs, S. O. Ferreira, E. Abramof, C. Boschetti, P. Motisuke, A. Y. Ueta, and I. N. Bandeira, J. Cryst. Growth **191**, 466 (1998).
[7] D. A. G. von Bruggeman, Ann. Phys. **24**, 636 (1935).
[8] P. Blaha, K. Schwarz, G. K. H. Madsen, D. Kvasnicka, and J. Luitz, WIEN2k, An Augmented Plane Wave + Local Orbitals Program for Calculating Crystal Properties (Karlheinz Schwarz, Techn. Universität Wien, Austria, 2001), ISBN 3-9501031-1-2.
[9] N. S. Dantas, A. Ferreira do Silva, and C. Persson, Opt. Mater., DOI: 10.1016/j.optmat.2007.09.001(2007).
[10] P. Villars and L. D. Calvert (eds.), Pearson's Handbook of Crystallographic Data for Intemetallic Phases, 2nd ed., Vol. 4 (ASM International, Ohio, 1996).
[11] G. Kresse and J. Hafner, Phys. Rev. B **47**, R558 (1993).
[12] C. Ambrosch-Draxl and J. O. Sofo, Comput. Phys. Commun. **175**, 1 (2006).
[13] M. Cardona and D. L. Greenaway, Phys. Rev. **133**, A1685 (1964).

